Accepted Manuscript

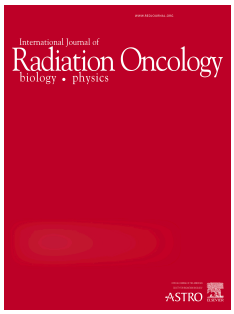

Automatic substitute CT generation and contouring for MRI-alone external beam radiation therapy from standard MRI sequences

Jason A. Dowling, Ph.D, Jidi Sun, M.Sc, Peter Pichler, M.P.H, David Rivest-Hénault, Ph.D, Soumya Ghose, Ph.D, Haylea Richardson, B.Med.Rad.Sc, Chris Wratten, FRANZCR, Jarad Martin, M.D, Jameen Arm, M.Sc, Leah Best, B.Sc, Shekhar S. Chandra, Ph.D, Jurgen Fripp, Ph.D, Frederick W. Menk, Ph.D, Peter B. Greer, Ph.D

PII: S0360-3016(15)03247-2

DOI: 10.1016/j.ijrobp.2015.08.045

Reference: ROB 23147

To appear in: *International Journal of Radiation Oncology • Biology • Physics*

Received Date: 19 May 2015

Revised Date: 5 August 2015

Accepted Date: 25 August 2015

Please cite this article as: Dowling JA, Sun J, Pichler P, Rivest-Hénault D, Ghose S, Richardson H, Wratten C, Martin J, Arm J, Best L, Chandra SS, Fripp J, Menk FW, Greer PB, Automatic substitute CT generation and contouring for MRI-alone external beam radiation therapy from standard MRI sequences, *International Journal of Radiation Oncology • Biology • Physics* (2015), doi: 10.1016/j.ijrobp.2015.08.045.

Automatic substitute CT generation and contouring for MRI-alone external beam radiation therapy from standard MRI sequences

Jason A. Dowling, Ph.D.[1,3*], Jidi Sun, M.Sc.[3], Peter Pichler M.P.H.[2], David Rivest-Hénault Ph.D.[1], Soumya Ghose Ph.D.[1], Haylea Richardson B.Med.Rad.Sc.[2], Chris Wratten, FRANZCR[2,3] , Jarad Martin M.D. [2,3], Jameen Arm M.Sc.[2], Leah Best B.Sc.[4], Shekhar S. Chandra Ph.D.[5], Jurgen Fripp Ph.D.[1], Frederick W Menk Ph.D.[3] Peter B. Greer Ph.D.[2,3]

1 CSIRO Australian e-Health Research Centre, Queensland, Australia

2 Calvary Mater Newcastle Hospital, New South Wales, Australia

3 University of Newcastle, New South Wales, Australia

4 Department of Radiology, Hunter New England Health, New South Wales, Australia

5 School of Info. Tech. and Electrical Engineering, University of Queensland, Australia

Corresponding author:

Jason A. Dowling

CSIRO Australian e-Health Research Centre

Level 5 UQ Health Science Building 901/16, Royal Brisbane and Women's Hospital,

Herston, QLD, 4029, Australia

Phone: +61 73253 3634, Fax: +617 3253 3690

Email: jason.dowling@csiro.au

Shortened Running Title:

Substitute CT for MRI-alone treatment planning

Acknowledgments:

This work was supported by Cancer Council New South Wales research grant RG11-05, the Prostate Cancer Foundation of Australia (Movember Young Investigator Grant YI2011) and Cure Cancer Australia.

Conflicts of Interest:

None.

Summary

Retrospective validation of MR-alone treatment planning with 39 patients is evaluated. Substitute CT (sCT) and contours were automatically generated for all patients. The suitability of the method for clinical practice was demonstrated by a mean error between the sCT and real CT data (within body contour) of 0.6±14.7 HU. The difference in point dose monitor units was mean 0.3±0.8%, with a 3D Gamma pass rate of 1.00±0.00 (2 mm/2%).

Anonymous 1

Abstract

Purpose: Validation of automatic substitute CT (sCT) scans generated from standard T2 weighted MR pelvic scans for MR-Sim prostate treatment planning.

Methods and Materials: A Siemens Skyra 3T MRI scanner with laser bridge, flat couch and pelvic coil mounts was used to scan 39 patients scheduled for external beam radiation therapy for localized prostate cancer. For sCT generation a whole pelvis MRI (1.6 mm 3D isotropic T2w SPACE sequence was acquired. Three additional small field of view scans were acquired: T2w, T2*w and T1w flip angle 80^0 for gold fiducials. Patients received a routine planning CT scan. Manual contouring of the prostate, rectum, bladder and bones was performed independently on the CT and MR scans. Three experienced observers contoured each organ on MRI allowing inter-observer quantification.

To generate a training database, each patient CT scan was co-registered to their whole pelvis T2w using symmetric rigid registration and structure guided deformable registration. A new multi-atlas local weighted voting method was used to generate automatic contours and sCT results.

Results: The mean error in Hounsfield units (HU) between the sCT and corresponding patient CT (within the body contour) was 0.6±14.7 (mean±1 SD) with a mean absolute

error of 40.5±8.2 HU. Automatic contouring results were very close to the expert inter-observer level (DSC): prostate 0.80±0.08, bladder 0.86±0.12, rectum 0.84±0.06, bones: 0.91±0.03 and body:1.00±0.003. The change in monitor units (MU) between the sCT-based plans relative to the gold standard CT plan for the same dose prescription was found to be 0.3±0.8%. The 3D Gamma pass rate was 1.00±0.00 (2 mm/2%).

Conclusions: The MR-Sim setup and automatic sCT generation methods using standard MR sequences generates realistic contours and electron densities for prostate cancer radiation therapy dose planning and DRR generation.

Key Words: Radiation therapy planning; prostate cancer; electron density; MRI, pseudo CT; substitute CT, synthetic CT

1 Introduction

Computed tomography (CT) scans are currently critical for image guided radiation therapy dose planning. CT allows a calibration relationship between voxel values and tissue electron density to be established for dose calculations, and the generation of digitally reconstructed radiographs (DRRs)[1]. However Magnetic Resonance Imaging (MRI) offers much improved soft tissue visualisation, does not expose a patient to ionizing radiation, and offers a number of functional imaging options[2]. Advantages of planning directly on MRI scans include reductions in costs and uncertainties introduced by the registration process[3]. Further motivation for MRI based substitute CT (sCT) scans (also known as synthetic or pseudo CT) are hybrid MRI-linear accelerator devices and MRI-PET attenuation correction[2,4–7]. A significant barrier to MRI-alone workflows however is that scans cannot be calibrated to electron density due to different imaging principals and therefore dose calculations cannot currently be performed.

Methods to estimate electron density information from MRI for both radiation therapy and attenuation correction need to consider geometric distortion, magnetic field inhomogeneities, gradient nonlinearity and patient-induced susceptibility[8]. Four main approaches have been developed:

1. *Bulk density assignment* involves setting a region within the MRI to a homogenous density (for example, water and bone)[5,9–14]. The region contouring is usually performed manually which is time consuming (especially for bone). The main advantage of the approach is

simplicity, however calculations may not be as accurate as CT and realistic DRRs are not able to be constructed.

2. *Registration and atlas based approaches* involve the rigid and deformable mapping of CT intensities onto a target MRI scan. One approach is to register a single CT to a target MRI [15] resulting in an sCT, however a single registration is unlikely to accurately map complex anatomy. More accurate approaches involving a training set of registered CT-MRI image pairs which are then combined into an average CT-MRI atlas which can be mapped to a new MRI scan[16,17]. Pairwise registration of each atlas MRI to a target MRI followed by fusion of the co-registered CT images to estimate HU generally improves accuracy[18,19]. Advantages of this approach involve the use of *a priori* geometric information and registration regularization to maintain realistic anatomical deformation. Atlas based approaches are currently the only fully automated methods for converting a single, standard MRI sequence to sCT and are more robust to intensity differences between images. The main disadvantage of are that the registration algorithms used may be unable to deform atlas images to match anatomical properties which are missing from an atlas-training set. Multiple pairwise registration can also be CPU-intensive, however the overall plausibility of the result is implicitly guaranteed.

3. *Regression, classification, or direct approaches* aim to characterize tissue properties directly from MR image intensities. As with atlas-based approaches, most regression methods rely on a training set of co-registered CT-MR scans to learn the intensity mapping[20]. Generally a minimum of three tissue classes (soft tissue, air and bone) are classified from one or more

MR images of the same patient anatomy[21,22]. Classes for water and fat may be added for increased accuracy[22–27] . A disadvantage of these approaches is the reliance on a combination of MRI sequences for tissue class differentiation and on research-only sequences such as ultra-short echo time (UTE). These sequences can significantly add to acquisition time and increase patient discomfort and motion. Advantages of these methods include execution speed and a potential increase in accuracy over atlases (reduction in registration error and greater robustness to abnormal anatomy), however it is difficult to guarantee the overall anatomical plausibility of the result.

4. *Hybrid approaches* have been proposed which combine both atlas and regression methods and show promise in sCT generation from a single, standard MRI sequence[20,28] .

This paper presents a retrospective study involving an MRI-simulator (with a flat couch top and coil mount to reduce body deformation). Results from a novel multi-atlas method using advanced registration techniques and local weighted voting to automatically map electron densities to standard MRI scans are presented. Multiple contoured patient MRI-CT sets are mapped to a patient and combined to create an accurate sCT with automatic structures. This sCT is then used for dose planning and DRR generation. Validation is performed by comparing doses calculated on the sCT with those on the planning CT. This approach should facilitate the introduction of MRI-alone prostate planning to routine clinical use as well as future MRI-based adaptive treatments.

2. Patients and Method

2.1 Patient Data Collection

Ethics approval for the study protocol was obtained from the local area health ethics committee and informed consent obtained from all patients. Patients were aged between 58-78 years, and all were diagnosed with tumours staged between T1-T3 (T1cN0M0 most common). BMIs ranged from 19.1-35.4. Each patient had three prostate pure gold fiducial markers of diameter 1.0x3.0 mm inserted trans-rectally by a urologist 1-2 weeks prior to the planning image acquisition. 42 patients in total were recruited, however the first three patient scans were acquired soon after commissioning the MRI scanner, and these scans were excluded due to an inadequate field of view for treatment planning and significant artefacts.

CT scans were acquired on a GE LightSpeedRT large bore scanner (2.5 mm slices) or a Toshiba Acquilion (2.0 mm slices). Patients were scanned with a full bladder and empty rectum. All patients followed a bowel preparation protocol (high fibre diet and daily Metamucil intake). Patients were positioned supine on a rigid couch-top with knee and ankle immobilisation stocks.

Four MRI sequences for each of the 39 patients were acquired with a Siemens Skyra 3T scanner. The scanner was equipped for MR simulation with a dedicated radiation therapy flat couch and coil mounts supplied by CIVCO (CIVCO Medical Solutions, Coralville, IA) and a laser bridge from LAP Lasers (LAP Laser, Luneburg, Germany). All patients were positioned by two radiation therapists. Only conventional MR scanning sequences were used. The planning MR was a 3D, T2

weighted 1.6 mm isotropic SPACE (Sampling Perfection with Application optimized Contrasts using different flip angle Evolution) sequence with field-of-view to cover the entire pelvis (including all of the bladder). The prostate delineation sequence was a 2D axial T2 weighted sequence with field-of-view approximately 200x200 mm^2. A further T1 weighted gradient echo sequence with flip angle 80 degrees was used to image intraprostatic gold seeds. A T2* scan was also acquired for the seeds (for a separate study validating the T1 weighted sequence). Patients were MR imaged prior to treatment as close as possible to the acquisition of the conventional planning CT scan. The parameters for each of these scans are summarised in Table 1.

Patient images were uploaded into the Eclipse treatment planning software (Varian Medical Systems, Palo Alto, CA, USA, version 11.0). Gold seed positions were localised on the T1 scan and transferred to the aligned T2 MRI image set as a structure contour. In standard CT based planning this image was then manually registered to the CT image set by alignment of the gold seed contours to visible gold seeds on the CT image set. Only translations in the x, y and z planes were applied.

To assess inter-observer contouring variability, the prostate (from the small field of view T2 scan), bladder and rectum (both from the whole pelvis T2 scan) for all patients were contoured independently by the same three observers (two experienced radiation oncologists and an experienced research radiation therapist). As in previous papers[29,30] we generated a gold standard contour for each organ using majority voting to combine the observer contours. The use of STAPLE[31] to combine these contours has previously been investigated (having no significant difference with voting[30]) and was not applied. The automatic segmentation tools from Varian

Eclipse were used for CT bone delineation and this contour was rigidly aligned to the whole pelvis MRI scan manually and adjusted by the research radiation therapist.

Seven field intensity modulated treatment delivery is used at our centre for prostate treatments. The treatments were delivered in 37-39 fractions of 2 Gy per fraction. The Clinical Target Volume (CTV, prostate) to Planning Target Volume (PTV) margin used was 7 mm.

2.2 Training data

All image analysis was performed in 3D. Before use the T2 scans were preprocessed with the following steps built using the Insight Segmentation and Registration Toolkit (ITK 4.4)[32]:

1. N4 Bias field correction[33] (B-spline fitting: [160, 3, 0, 0, 5], convergence: [100x100x100, 0, 0.001], shrink factor: 3).
2. Histogram equalization (levels: 1024, match points: 7, threshold at mean intensity).
3. Smoothing via gradient anisotropic diffusion (10 iterations, time step: 0.03; conductance: 1.0).

To generate a training database, each patient CT scan was co-registered to their whole pelvis T2 with a robust symmetric rigid registration[34,35] followed by structure guided deformable registration (to promote bone rigidity while allowing high quality bladder and rectum registration[36]).

2.3 Conversion of a new patient MRI

A multi-atlas local weighted voting method, based on a method applied by Artaechevarria et al.[37] to brain scans was used to generate sCT and automatic contouring results for each target MRI scan. This method involves five main steps:

1. All whole pelvis MRI scans (n=38, as leave-one-out) in the training database were registered to the target MRI using symmetric rigid[34] followed by diffeomorphic demons registration [38]. Note that structure guided registration is not used here as structures are not available on the target MRI. The rigid transform and deformation field from each of the 38 pairwise registrations were then also applied to binary images representing structures generated from contours from each training MRI.
2. A patch around each voxel (radius=2 voxels) in the target MRI was compared with patches in the same location on the registered MRI images and a similarity metric computed (sum of squared differences). The weights for each voxel on all registered MR images were then normalized to one.
3. The normalized similarity for each voxel was then used as a weighting to generate the estimated HU from the same voxels in the co-registered CT's. Each voxel in the sCT image is therefore generated from the same voxel in each registered CT-MR image which has been weighted to match the MRI neighbourhood.
4. The same weights were similarly used to determine the spatial locations for each binary image (representing structures).

5. Standard MRI sequences have reduced capacity to extract signal from tissues with shorter echo times. A small systematic difference in the body contour on MRI and CT for each patient was observed representing missing signal from collagen. A 1mm expansion was added to the sCT to account for this missing outer skin layer. The dilated skin was assigned a value of 47 HU based on sampling of this area on the planning CT. The automatic body contour was expanded in the same way.
6. The generated sCT and structures (converted from binary images) were output to a DICOM-RT directory[39].

2.4 Validation

A leave-one-out approach was used. In this testing methodology, to avoid biasing results, each sCT is generated without data from the patient being tested. Therefore 38 patient scans were used to generate each sCT, and to evaluate organ segmentation accuracy.

The quality of the sCT conversion was assessed in three ways: direct comparison of voxel intensity differences between the sCT and the CT (mean and mean absolute errors); differences in dose distributions; and automatic contour accuracy.

To evaluate dose differences, the sCT images were imported into the corresponding patient record in the treatment planning system. The existing CT based treatment plans including the CT defined structures for each patient were then copied and attached to the sCT images (using bone for initial alignment, then further refinement based on the fiducial markers according to the clinical protocol).

To evaluate dose differences, the dose at the ICRU point, 3D gamma evaluation, and dose-volume histogram (DVH) parameters for the planning target volume (PTV) were compared.

The automatic contours were compared against the manual contours using the Dice Similarity Coefficient (DSC = 2 (A ∩ B / (A ∪ B)) and the mean absolute surface distance (MASD) which is calculates the average absolute Euclidean distance between surfaces (ITK, ContourMeanDistanceImageFilter class).

3. Results

The mean error in HU between the sCT and matching patient CT data (within the patient's body contour) was 0.6±14.7 (mean±1 SD). The mean absolute error within the same contour was 40.5±8.2 HU. Figure 1 shows the automatically generated sCT, the original CT (registered to the patient's MRI) and the difference between the estimated and actual CT volumes from one study patient (number 6).

With a 2 Gy prescribed dose at the ICRU point, the change in monitor units (MU) was used to compare the dose change for the plans using sCT images relative to the gold standard CT plan. A reference ICRU dose point was created on the CT dose distribution and then the same point was transferred to the sCT. The percentage difference of the dose calculated at the reference point between the two plans was -0.3±0.8%, range [-1.5, 1.8].

3D gamma analysis was also used to evaluate dose. This evaluation method includes both dose-difference (DD) and distance-to-agreement (DTA) criteria[40]. In this study 3D gamma analysis was performed with global dose criteria of 2mm/2% (DTA/DD) and 1mm/1%. The dose distribution calculated on the CT plan was considered the reference, while the sCT plan dose distribution was considered the evaluated quantity. The dose matrices were exported from Varian Eclipse. The two dose images were aligned (Matlab, MathWork) based on the isocentre location in each image, as the CT and MR images were already registered in Eclipse. The sCT plan dose matrix was then interpolated to the reference CT plan dose matrix. Finally, the 3D gamma analysis was performed using inhouse Matlab code (Figure 2). Three different dose thresholding approaches were used, a 90% threshold capturing dose within the PTV region (P), a global 10% threshold capturing dose within the entire body contour (B), and a morphological erosion operation was applied to exclude the body surface (~15mm) where gamma failures occur due to small differences in the body contour of CT and sCT (B').

The dose distributions on CT and sCT were also compared using DVH parameters (D90%, D50% and D5%). The mean ± std (25%, 75% quartiles) of the CT and sCT DVH parameter differences (sCT-CT) were calculated as ΔD95% = -0.3±1.1 (-0.9, 0.2); ΔD50%=-0.5±1.1 (-1.4, -0.0); ΔD5% = -0.4±1.2 (-1.3, 0.0). No significant differences were found (t-test, α=0.05) for D95% (p=0.1792), D50% (p=0.0503) and D5% (p=0.1646). Dosimetric results (dose comparison, gamma, and DVH) for the best and worst patient gamma scores are visually shown in Figures 3 and 4.

The automatic bone contours on the MR scans were very accurate with a DSC of 0.91±0.03 and MASD of 1.45±0.47 mm. Mean automatic organ contouring results compared to manual contours were all above 0.8 DSC and were close to the inter-observer level (Table 2).

4. Discussion

The results presented in this paper compare favourably with previous literature on sCT generation for MR-alone prostate radiation therapy planning. Chen et al.[41] applied a bulk density approach and found dose difference between sCT and planning CT of 2.5%. Using an automatic average atlas approach Anonymous et. al[16] reported a point dose difference between sCT and planning CT of 1.3%. Korhonen et al.[42] used manual bone contouring, and a regression approach and achieved an absolute difference of 11±9 HU and for soft tissue and 99±100 HU for bony tissue for 10 patients. They reported high gamma agreement using a single axial plane 2D evaluation for 7 field IMRT treatments with 2%,2mm criteria of 99.6±0.3%. DVH parameter agreements (D95%, D50% and D5%) were 0.3±0.2%. For these comparisons the CT and sCT body contours were adjusted to be equivalent. Kim et al.[18] reported for a semi-automatic (bone needed to be manually contoured) method a MAE of 74 HU and mean dose difference of 0.75%. In this paper we have described a fully automatic method to achieve an MAE of 40±8.2 HU with a mean dose difference of 0.3±0.8% for a large patient dataset. Gamma analysis and DVH parameter comparisons demonstrates that the dose distribution for all patients were in a high level of agreement. In this work there was no normalization of the body contour between CT and sCT therefore the most Gamma failures occurred at the body surface region where there were differences in contour, (dose was present in

one scan but not the other). Gamma calculations were therefore also performed excluding this region. There is currently no consensus on how to evaluate sCT dose distributions compared to CT so we have used the most commonly reported evaluation metrics (MAE HU, point dose, Gamma and DVH parameters).

Our method has been developed with a standard clinical workflow in mind and does not rely on specialised sequences, or manual bone contouring. The automatic MRI bone contours were found to have a high level of accuracy which will be important in the clinical workflow to assess doses to these structures.

Previous work from our group has reported that geometric distortion within our MR-Sim setup was found to be accurate, with organ dimensions, dose distributions and DRR based setup within acceptable limits compared to CT [43]. The MRI coil mount reduces body deformation but has an impact on image quality (the coil needs to be positioned with a minimal and uniform body-to-coil distance in order to maximize image quality)[44].

Requirements for accurate sCT conversion include carefully matching the patient position between CT and MR for training data, MR scans with an adequate field of view to match a standard planning CT and high quality sequence acquisition (preferably isotropic voxels). Accurate co-registration of CT-MR scans (preferably using structure guided registration) is a critical step in developing training data for sCT generation.

5. Conclusions

This study has shown that substitute CT scans can be automatically generated from MR scans using conventional T2 weighted sequences and that dose calculations are comparable to conventional CT scan dose calculations. The MR-only workflow is efficient and only requires one imaging session for the patient.

A major advantage of the technique is that it does not require specialized or research sequences (such as UTE), and only a single sequence is required for substitute CT generation, decreasing scanning time and potential patient motion.

References

1. Khan FM. *The Physics of Radiation Therapy*. 4th ed. Lippincott Williams & Wilkins; 2009. Available at: http://www.amazon.com/dp/0781788560.

2. Lagendijk JJW, Raaymakers BW, Van den Berg CAT, Moerland MA, Philippens ME, van Vulpen M. MR guidance in radiotherapy. *Phys Med Biol*. 2014;59(21):R349-69. doi:10.1088/0031-9155/59/21/R349.

3. Nyholm T, Jonsson J. Counterpoint: Opportunities and challenges of a magnetic resonance imaging-only radiotherapy work flow. *Semin Radiat Oncol*. 2014;24(3):175-80. doi:10.1016/j.semradonc.2014.02.005.

4. Karlsson M, Karlsson MG, Nyholm T, Amies C, Zackrisson B. Dedicated magnetic resonance imaging in the radiotherapy clinic. *Int J Radiat Oncol Biol Phys*. 2009;74(2):644–651.

5. Lee YK, Bollet M, Charles-Edwards G, et al. Radiotherapy treatment planning of prostate cancer using magnetic resonance imaging alone. *Radiother Oncol*. 2003;66(2):203–216.

6. Glide-Hurst CK, Wen N, Hearshen D, et al. Initial clinical experience with a radiation oncology dedicated open 1.0T MR-simulation. *J Appl Clin Med Phys*. 2015;16(2). doi:10.1120/jacmp.v16i2.5201.

7. Anonymous

8. Kim J, Glide-Hurst C, Doemer A, Wen N, Movsas B, Chetty IJ. Implementation of a Novel Algorithm For Generating Synthetic CT Images From Magnetic Resonance Imaging Data Sets for Prostate Cancer Radiation Therapy. *Int J Radiat Oncol Biol Phys*. 2015;91(1):39-47. doi:10.1016/j.ijrobp.2014.09.015.

9. Beavis AW, Gibbs P, Dealey RA, Whitton VJ. Radiotherapy treatment planning of brain tumours using MRI alone. *Br J Radiol*. 1998;71(845):544-8. doi:10.1259/bjr.71.845.9691900.

10. Chen LL, Price RA, L. Wang L. et al. MRI-based treatment planning for radiotherapy: dosimetric verification for prostate IMRT. *Int J Radiat Oncol Biol Phys*. 2004;60(2):636-647.

11. Chin AL, Lin A, Anamalayil S, Teo B-KK. Feasibility and limitations of bulk density assignment in MRI for head and neck IMRT treatment planning. *J Appl Clin Med Phys*. 2014;15(5):4851. Available at: http://www.ncbi.nlm.nih.gov/pubmed/25207571. Accessed December 17, 2014.

12. Eilertsen K. A simulation of MRI based dose calculations on the basis of radiotherapy planning CT images. *Acta …*. 2008;47(7):1294-1302. doi:10.1080/02841860802256426.

13. Prabhakar R, Julka PK, Ganesh T, Munshi A, Joshi RC, Rath GK. Feasibility of using MRI alone for 3D Radiation Treatment Planning in Brain Tumors. *Jpn J Clin Oncol*. 2007;37(6):405-411. doi:10.1093/jjco/hym050.

14. Anonymous

15. Wang C, Chao M, Lee L, Xing L. MRI-based treatment planning with electron density information mapped from CT images: a preliminary study. *Technol Cancer Res Treat*. 2008;7(5):341-348. Available at: http://www.ncbi.nlm.nih.gov/pubmed/18783283.

16. Anonymous.

17. Stanescu T, Jans H-S, Pervez N, Stavrev P, Fallone BG. A study on the magnetic resonance imaging (MRI)-based radiation treatment planning of intracranial lesions. *Phys Med Biol*. 2008;53(13):3579-93. doi:10.1088/0031-9155/53/13/013.

18. Kim J, Glide-Hurst C, Doemer A, Wen N, Movsas B, Chetty IJ. Implementation of a Novel Algorithm For Generating Synthetic CT Images From Magnetic Resonance Imaging Data Sets for Prostate Cancer Radiation Therapy. *Int J Radiat Oncol*. 2014. doi:10.1016/j.ijrobp.2014.09.015.

19. Burgos N, Cardoso MJ, Thielemans K, et al. Attenuation correction synthesis for hybrid PET-MR scanners: application to brain studies. *IEEE Trans Med Imaging*. 2014;33(12):2332-41. doi:10.1109/TMI.2014.2340135.

20. Hofmann M, Bezrukov I, Mantlik F, et al. MRI-based attenuation correction for whole-body PET/MRI: quantitative evaluation of segmentation- and atlas-based methods. *J Nucl Med*. 2011;52(9):1392-9. doi:10.2967/jnumed.110.078949.

21. Catana C, van der Kouwe A, Benner T, et al. Toward implementing an MRI-based PET attenuation-correction method for neurologic studies on the MR-PET brain prototype. *J Nucl Med*. 2010;51(9):1431-8. doi:10.2967/jnumed.109.069112.

22. Keereman V, Fierens Y, Broux T, De Deene Y, Lonneux M, Vandenberghe S. MRI-based attenuation correction for PET/MRI using ultrashort echo time sequences. *J Nucl Med*. 2010;51(5):812-8. doi:10.2967/jnumed.109.065425.

23. Berker Y, Franke J, Salomon A, et al. MRI-based attenuation correction for hybrid PET/MRI systems: a 4-class tissue segmentation technique using a combined ultrashort-echo-time/Dixon MRI sequence. *J Nucl Med*. 2012;53(5):796-804. doi:10.2967/jnumed.111.092577.

24. Edmund JM, Kjer HM, Van Leemput K, Hansen RH, Andersen J Al, Andreasen D. A voxel-based investigation for MRI-only radiotherapy of the brain using ultra short echo times. *Phys Med Biol*. 2014;59(23):7501-19. doi:10.1088/0031-9155/59/23/7501.

25. Hsu S-H, Cao Y, Huang K, Feng M, Balter JM. Investigation of a method for generating synthetic CT models from MRI scans of the head and neck for radiation therapy. *Phys Med Biol*. 2013;58(23):8419-35. doi:10.1088/0031-9155/58/23/8419.

26. Korhonen J, Kapanen M, Sonke J-J, et al. Feasibility of MRI-based reference images for image-guided radiotherapy of the pelvis with either cone-beam computed tomography or planar localization images. *Acta Oncol*. 2014:1-7. doi:10.3109/0284186X.2014.958197.

27. Jonsson JH, Johansson A, Söderström K, Asklund T, Nyholm T. Treatment planning of intracranial targets on MRI derived substitute CT data. *Radiother Oncol*. 2013;null(null). doi:10.1016/j.radonc.2013.04.028.

28. Gudur MSR, Hara W, Le Q-T, Wang L, Xing L, Li R. A unifying probabilistic Bayesian approach to derive electron density from MRI for radiation therapy treatment planning. *Phys Med Biol*. 2014;59(21):6595-606. doi:10.1088/0031-9155/59/21/6595.

29. Anonymous.

30. Klein S, Heide UA van der, Lips IM, Vulpen M van, Staring M, Pluim JPW. Automatic segmentation of the prostate in 3D MR images by atlas matching using localized mutual information. *Med Phys*. 2008;35(4):1407-1417.

31. Warfield SK, Zou KH, Wells WM. Simultaneous truth and performance level estimation (STAPLE): an algorithm for the validation of image segmentation. *IEEE Trans Med Imaging*. 2004;23(7):903–921.

32. Ibanez L, Schroeder W. *The ITK Software Guide 2.4*. Kitware, Inc.; 2005.

33. Tustison NJ, Avants BB, Cook PA, et al. N4ITK: Improved N3 Bias Correction. *Med Imaging, IEEE Trans*. 2010;29(6):1310-1320. doi:10.1109/TMI.2010.2046908.

34. Anonymous.

35. Anonymous.

36. Anonymous.

37. Artaechevarria X, Munoz-Barrutia A, Ortiz-de-Solorzano C. Combination strategies in multi-atlas image segmentation: application to brain MR data. *IEEE Trans Med Imaging*. 2009;28(8):1266-77. doi:10.1109/TMI.2009.2014372.

38. Vercauteren T, Pennec X, Perchant A, Ayache N. Diffeomorphic demons: efficient non-parametric image registration. *Neuroimage*. 2009;45(1 Suppl):S61-72.

39. Anonymous.

40. Low DA, Harms WB, Mutic S, Purdy JA. A technique for the quantitative evaluation of dose distributions. *Med Phys*. 1998;25(5):656-61. Available at: http://www.ncbi.nlm.nih.gov/pubmed/9608475. Accessed April 15, 2015.

41. Chen L, Price RA, Nguyen T-B, et al. Dosimetric evaluation of MRI-based treatment planning for prostate cancer. *Phys Med Biol*. 2004;49(22):5157–5170.

42. Korhonen J, Kapanen M, Keyriläinen J, Seppälä T, Tenhunen M. A dual model HU conversion from MRI intensity values within and outside of bone segment for MRI-based radiotherapy treatment planning of prostate cancer. *Med Phys*. 2014;41(1):011704. doi:10.1118/1.4842575.

43. Anonymous.

44. Anonymous.

Figures

Figure 1: Column A: Original MRI from study participant six. B: generated sCT, C: original patient CT. D shows the MAE between B and C.

Figure 2: Gamma evaluation results comparing the original CT plan to the same plan recalculated on the sCT scan. P=Prostate, B=Body, B'=Body with skin surface removed.

Figure 3: Results for patient 10 (best gamma result). A: original patient CT scan with dose plan overlaid. B: Estimated sCT for this patient (PTV contoured in blue). The gamma map (2mm/2%, body) is shown in C. D shows the DVH results (the dashed line with stars is from the sCT and the solid line with circles is the actual CT).

Figure 4: Results for study patient 36 (worst gamma result). Same layout as Figure 3. Note the significant difference in rectal air and prostate position.

Table 1. MRI Acquisition parameters*.

	T2 SFOV	T2 LFOV	T2*	T1
Scan Type	2D Axial TSE	3D SPACE TSE	GRE	GRE
TE (ms)	97	102	12	6.6
TR (ms)	1400	1200	689	689
Flip Angle (°)	135	135	25	80
FOV (mm)	200	430	200	200
Slice Thickness (mm)	2	1.56	2	2

Abbreviations: SFOV=small field of view; LFOV=large field of view; TSE=turbo spin echo; GRE=gradient echo; TE=echo time; TR=repetition time.

*Scans were created with a Siemens Skyra 3.0 Tesla magnet.

Table 2. Dice Similarity Coefficient (DSC) and Mean Absolute Surface Distance (MASD) results for automatic organ contouring compared to gold standard (fused) expert manual contours. The middle column shows the inter-observer overlap between the three experts for each organ. The final column shows the mean error (ME) and mean absolute error (MAE) of HU estimates within each automatic contour.

	Automatic vs manual contour		**Inter-observer (n=3) overlap**		**Difference between sCT and CT within automatic contour**	
	DSC	**MASD (mm)**	**DSC**	**MASD (mm)**	**ME (HU)**	**MAE (HU)**
Body	1.00±0.00	0.55±0.56	N/A	N/A	-0.56±14.17	40.45±8.16
Bones	0.91±0.03	1.45±0.47	N/A	N/A	-6.43±46.47	134.24±24.04
Bladder	0.86±0.12	5.10±4.57	0.95 ± 0.01	0.91±0.29	-2.9±18.71	24.05±13.62
Rectum	0.84±0.06	2.37±1.34	0.82 ± 0.07	2.64±1.55	6.86±81.72	88.07±60.81
GTV	0.80±0.08	2.30±1.01	0.84 ± 0.11	1.98±1.59	-0.47±11.82	16.47±4.50

Patient 10

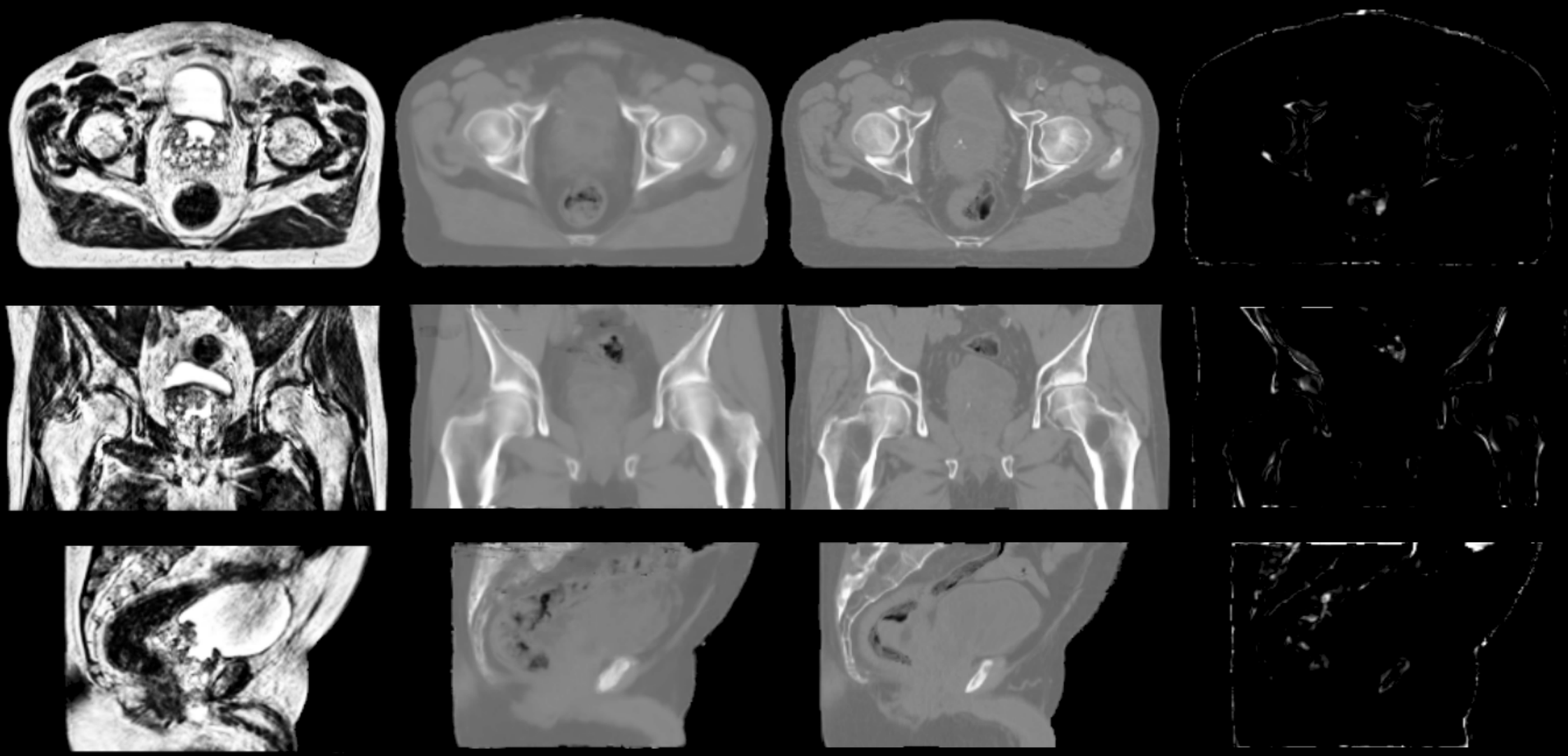

Patient 36

A. T2w MRI **B. sCT from MRI** **C. Planning CT** **D. Difference**

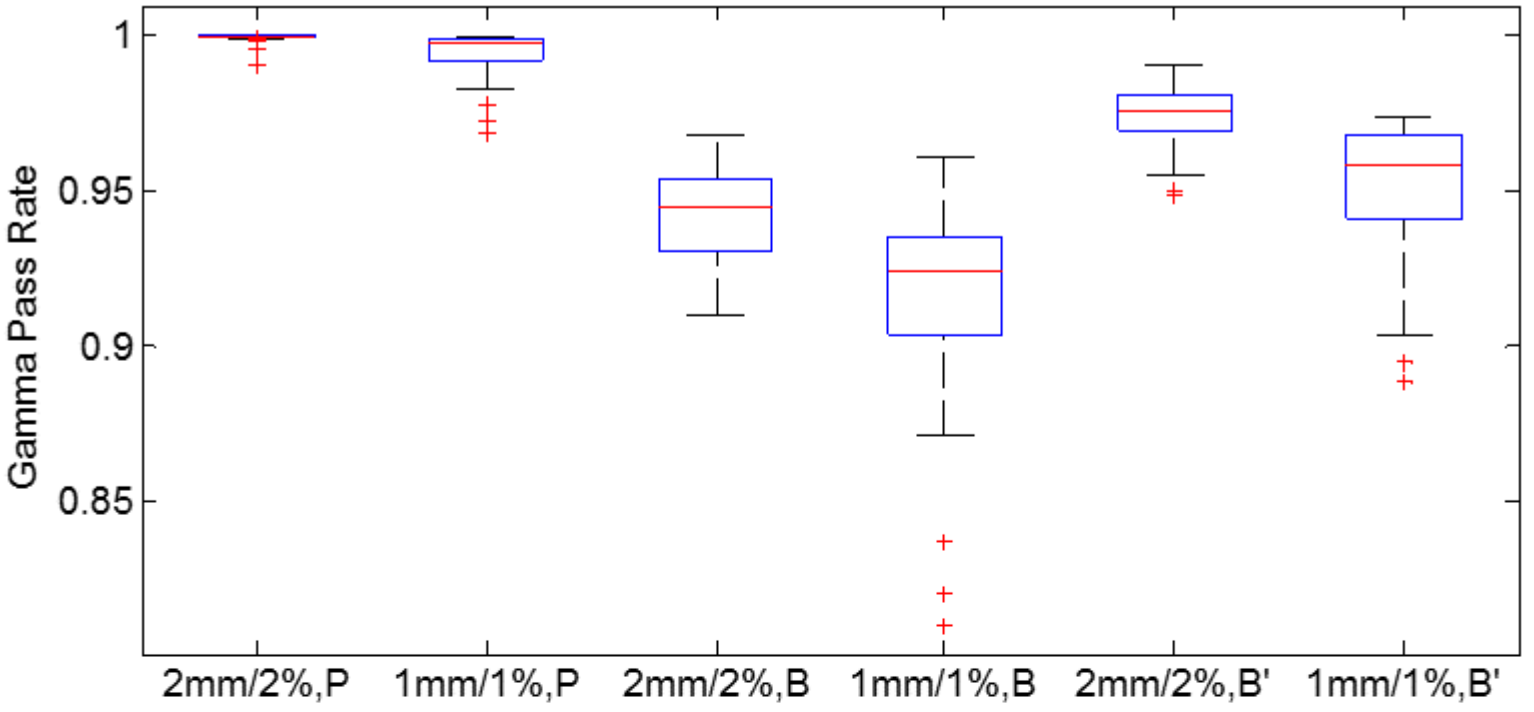
Gamma Pass Rate
1
0.95
0.9
0.85
2mm/2%,P
1mm/1%,P
2mm/2%,B
1mm/1%,B
2mm/2%,B'
1mm/1%,B'

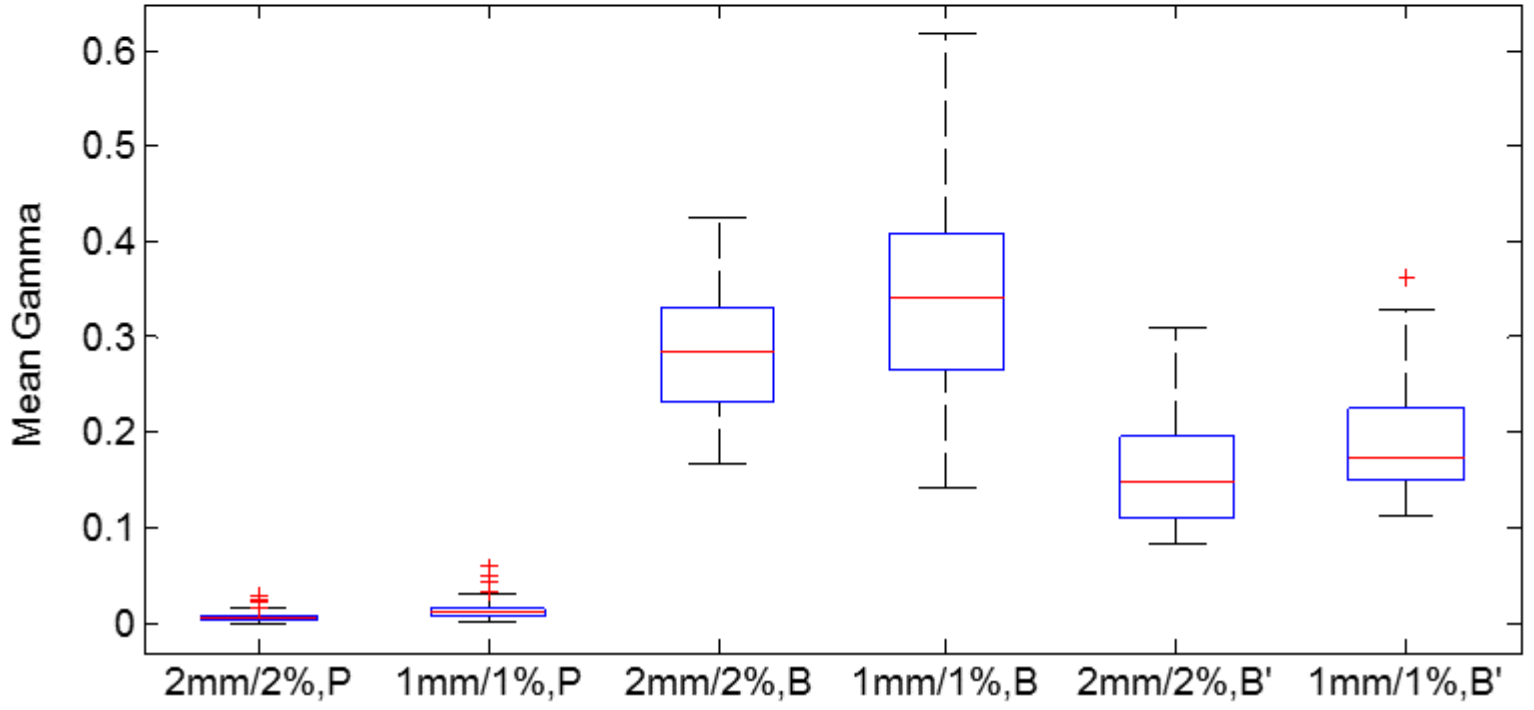
Mean Gamma
0.6
0.5
0.4
0.3
0.2
0.1
0
2mm/2%,P
1mm/1%,P
2mm/2%,B
1mm/1%,B
2mm/2%,B'
1mm/1%,B'

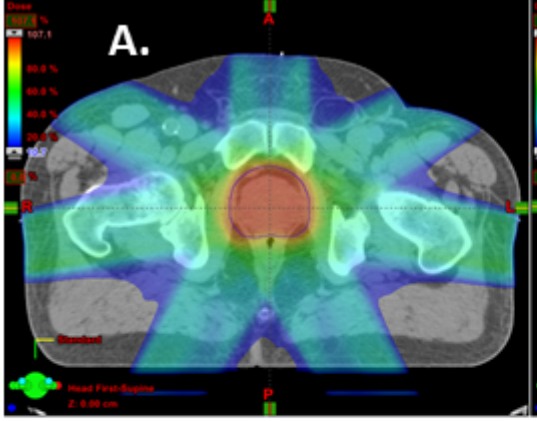
A.

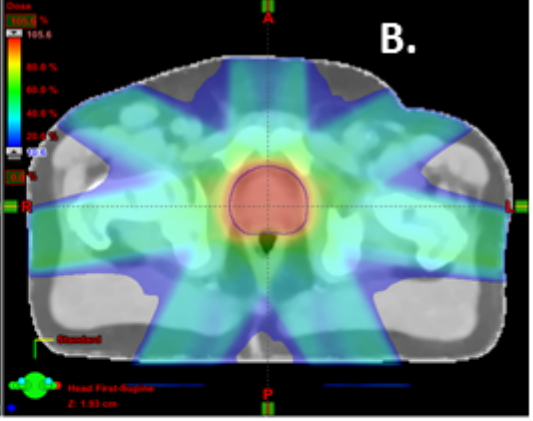
B.

C.

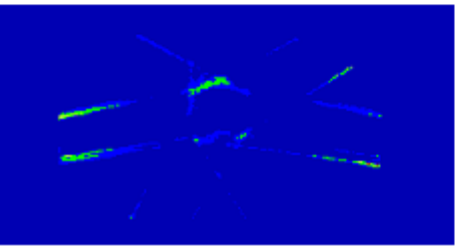

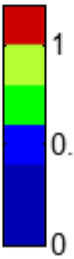
1
0.5
0

D.

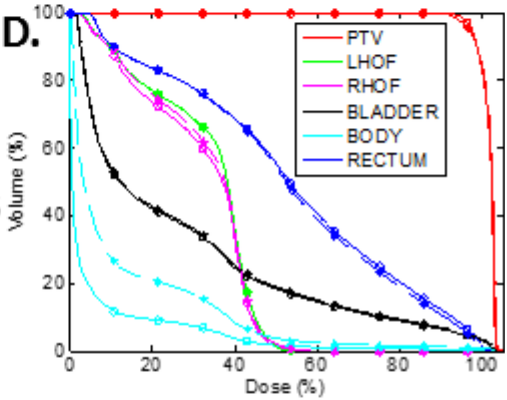
PTV
LHOF
RHOF
BLADDER
BODY
RECTUM
Volume (%)
Dose (%)
0
20
40
60
80
100

E.

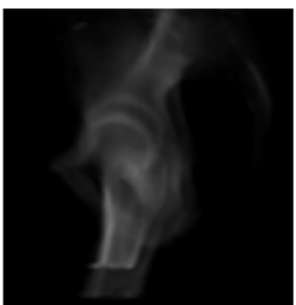

F.

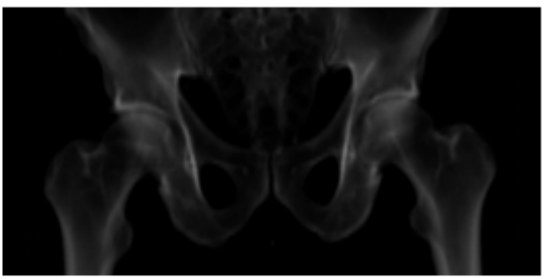

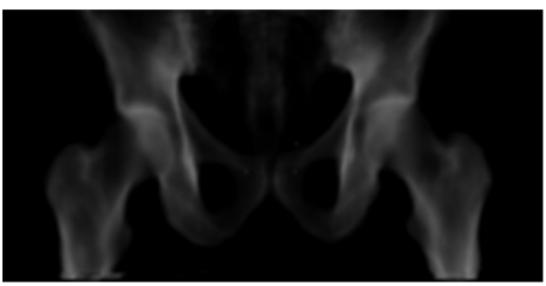

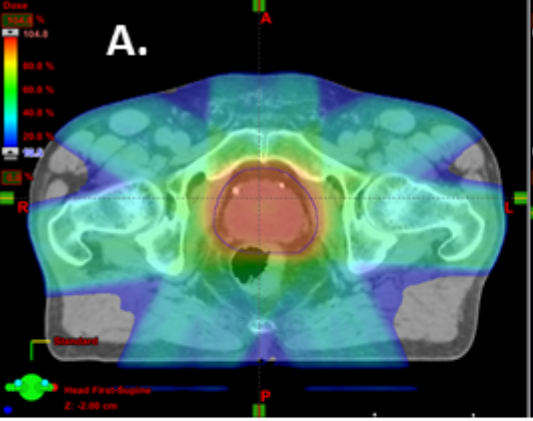
A.

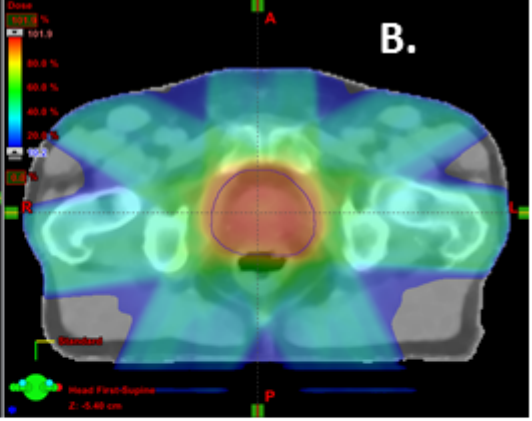
B.

C.

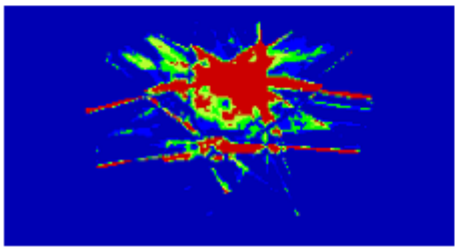

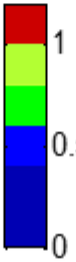
1
0.5
0

D.

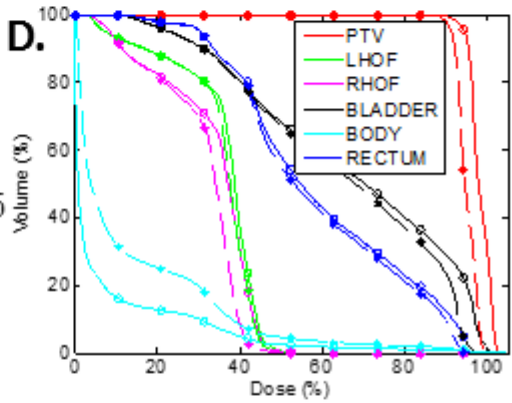
PTV
LHOF
RHOF
BLADDER
BODY
RECTUM
Volume (%)
Dose (%)
0
20
40
60
80
100

E.

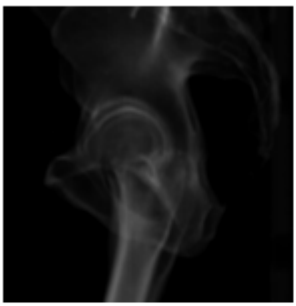

F.